Chemical Stability via Radical Decomposition Using Silicotungstic Acid Moieties for Polymer Electrolyte Fuel Cells

Andrew R. Motz,[1,*] Mei-Chen Kuo,[1] Guido Bender,[2,*] Bryan S. Pivovar,[2,*] and Andrew M. Herring [1,*,z]

[1] *Department of Chemical and Biological Engineering, Colorado School of Mines, Golden, Colorado 80401, USA*
[2] *National Renewable Energy Laboratory, Hydrogen & Fuel Cell Research, Golden, Colorado 80401, USA*

Chemical degradation of perfluorinated sulfonic acid membranes, such as Nafion, via radical attack, represents one of the current challenges of fuel cell durability. Here we report on a recent breakthrough in chemical durability that has been achieved through using covalently attached heteropoly acid (HPA) moieties as both the proton conducting acid and the radical decomposition catalyst. Exceptional chemical durability is reported for a thin (25 μm) film in an accelerated stress test that eventually had an open circuit voltage decay rate of 520 μV h^{-1}, which was shown to be a result of the formation of an electrical short after thinning due to mechanical stresses. A mechanism is proposed using density functional theory in which the W atoms in the HPA reversibly change oxidation state from W(VI) to W(V) while decomposing radical species. Using rate constants found in the literature and realistic concentrations of scavenging species, it is hypothesized that the rate of radical decomposition can be >35x faster for HPA containing membranes than it is for Ce doped films. It is concluded that covalently tethered HPA should be considered as a next generation chemical stabilization strategy for polymer electrolyte fuel cells.

 [DOI: 10.1149/2.1361814jes]

Manuscript submitted August 14, 2018; revised manuscript received November 8, 2018. Published November 20, 2018. This was Paper 1465 presented at the Cancun, Mexico, Meeting of the Society, September 30–October 4, 2018.

Fuel cells are energy conversion devices that have the potential to power fuel cell electric vehicles, representing a cleaner and more sustainable alternative to internal combustion engines.[1] Fuel cell technology is being released on a limited basis in vehicles and has had success in materials handling, a niche market where fuel cells have many advantages.[2,3] For the wide spread adoption of fuel cell technology, performance and durability need to improve while cost is reduced. Use of thinner membranes reduces ohmic losses, simplifies water management, and saves material cost, but these benefits come at the detriment of membrane durability.[4]

Two main membrane degradation mechanisms have been identified, chemical and mechanical, and there is an expected interplay between the two mechanisms that is still not fully understood.[5–7] Mechanical degradation derives from cycling humidity. Polymer electrolytes have a water sorption isotherm (and subsequent volume change) that is highly dependent on relative humidity and when subjected to humidity cycling, swelling and subsequent mechanical stress causes membrane degradation. While there is potential for improvement in the mechanical durability of membranes, addition of expanded polytetrafluoroethylene (ePTFE) is seen as a sufficient solution, as the perfluorosulfonic acid polymer (PFSA)/ePTFE composites have reduced in-plane swelling, improved mechanics, and are more resistant to electrical shorts.[8] Currently, the chemical stability of PFSA is not sufficient. Chemical degradation occurs via radical attack throughout the catalyst layers and the membrane, where the radical species in the membrane are the result of hydrogen peroxide decomposition.[9,10] The •OH radicals are responsible for unzipping polymer chains through reaction with carboxylic acid end groups where •H radicals are potentially responsible for the slower, but more detrimental main chain cleavage.[11,6] It is worth noting that when O_2 is present, rapid, diffusion controlled reaction with •H will form •OOH and the lifetime of •H has been approximated to be on the order of 10 ns.[12] The •OOH radical, though present, has been shown to be much less reactive.[12,9] Membranes produced from PFSA polymers, treated with elemental fluorine, and doped with Ce^{3+} and Mn^{2+} are the state of the art materials, but two main drawbacks to using Ce^{3+} or Mn^{2+} as a radical scavenger exist. First, is the displacement of mobile protons and the second limitation is the migration of the radical scavenging species.[13–15] It has recently been reported that the pre-commercial, perfluorosulfonyl imide acid polymer (PFIA) material being developed at 3M suffers from similar chemical degradation in open circuit voltage (OCV) tests, but the mechanism is more complex due to the longer, multi-acid side chain with more potential sites for radical attack.[16] Hydrocarbon membranes react more readily with radical species and thus require a better mitigation strategy than is currently available for practical levels of durability, but some hydrocarbon materials with very low oxygen crossover are able to achieve respectable OCV decay rates.[17,18]

Heteropoly acids (HPAs), a subclass of polyoxometalates, are another class of radical scavenging molecules.[6] Several types of HPAs have demonstrated the ability to improve membrane chemical stability through polymer blends, but they still suffer from migration and only result in marginal gains.[19,20] A method of covalent bonding HPAs to carbon in the catalyst layer has also shown some improvements in chemical stability, but chemical degradation mitigation within the membrane is needed.[21,22] Our group has developed two membrane platforms with HPAs covalently attached and immobilized within a polymer membrane, serving as the proton conducting acid.[23–26] More recently, the outstanding chemical stability of one of these platforms has been demonstrated,[26] however, the stability demonstrated in this study was criticized for using rather thick, 80 μm membranes in subscale fuel cells.

In this study a 50 cm^2 fuel cell was fabricated using a thin, 25 μm membrane with covalently attached silicotungstic acid, which was subjected to an accelerated stress test for chemical degradation and displayed an OCV decay rate of 520 μV h^{-1}. To the authors knowledge, this is the first reported fuel cell of a larger practical area containing a hybrid HPA film and represents a significant step toward demonstrating this technology on a commercially relevant scale. The resulting data was analyzed to show the loss in OCV is mainly due to an electrical short and not increased reactant gas crossover. This study further analyzes the chemical stability observed in these membranes and proposes a mechanism for radical decomposition. A reaction mechanism is proposed utilizing reactions found in literature as well as density functional theory (DFT) calculations. The main conclusion from this work is that covalently attached HPAs could be more efficient radical scavengers with less susceptibility to migration, accumulation, and leaching when compared to the use of Ce(III) cations.

Materials and Methods

Synthesis.—The silicotungstic acid (HSiW) functionalized poly(vinylidene fluoride-co-hexafluoropropylene) (PolyHPA)

*Electrochemical Society Member.
[z]E-mail: aherring@mines.edu

membrane was synthesized as previously reported and contained 70 wt% $K_8SiW_{11}O_{39}$.[26] The membrane was cast from solution in N, N dimethylacetamide on a Kapton liner, dried at room temperature, and annealed under 4000 psi at 160°C for 5 min. The film was subsequently removed from the Kapton liner through immersion in water and ion-exchanged via soaking in 1M H_2SO_4 three times. The film was then rinsed with water until the pH was >6.0. The resulting film was 25 μm thick.

Fuel cell fabrication.—A 50 cm^2 square fuel cell was fabricated using Johnson Matthey ELE0162 gas diffusion electrodes (GDEs) with a geometric platinum loading of 0.35 mg Pt cm^{-2} for both the anode and cathode. Two Teflon gaskets and a polyethylene sub gasket were used. The cell was assembled with a two-channel anode and a three-channel cathode graphite flow field in fuel cell hardware and the bolts were torqued to 10 ft-lb. To avoid membrane fracture, the membrane electrode assembly did not undergo a thermal adhesion step under pressure.

Fuel cell testing.—The membrane was broken in at 80°C, saturated inlet gases, and 0.4 V for 30 min prior to collection of an IV curve under the same conditions. The cell was then ramped to 90°C and 30%RH and nitrogen was supplied to the cathode. Linear sweep voltammetry (LSV) was performed with a scan rate of 0.1 mV s^{-1} from OCV to 0.5 V. Next an accelerated stress test (AST), was performed as follow: air was supplied to the cathode and high frequency resistance (HFR) was collected at 0.6 V. After the HFR measurement, the cell was held at OCV for 20–72 h. After the OCV hold, the LSV and HFR measurements were repeated, followed by the next OCV hold. This process was repeated until the duration of the OCV hold was an accumulated 500 h.

Density functional theory calculations.—The DFT calculations were performed using the M062X level of theory with LANLDZ basis sets, as implemented by the Gaussian09 software package using an extra fine grid.[27–29] First, the $SiW_{12}O_{40}^{-4}$ anion was optimized, starting with the experimentally determined crystal structure.[30] Next, the structures for $SiW_{12}O_{40}H^{-4}$ ($[SiW_{12}O_{40}^{-4}]$-H) and $SiW_{12}O_{40}OH^{-4}$ ($[SiW_{12}O_{40}^{-4}]$-OH) were optimized through adding an H and an OH, respectively, to a terminal oxygen of the optimized $SiW_{12}O_{40}^{-4}$ anion. The multiplicity of both $[SiW_{12}O_{40}^{-4}]$-H and $[SiW_{12}O_{40}^{-4}]$-OH was m = 2. For enthalpic and geometric comparison, •H, •OH, •OOH, H_2, H_2O, and H_2O_2 structures were optimized using M062X/ LANLDZ. A frequency calculation for all of the structures resulted in only positive, real frequencies indicating that all structures were a local energy minimum.

Results and Discussion

Open circuit voltage (OCV) hold accelerated stressed test (AST) results.—A recent study has highlighted the chemical stability of a polymer electrolyte containing HPA moieties of the Keggin structure, see structure of PolyHPA in Figure 1.[26] This current study further investigates this chemical stability using films of a more practically relevant thickness and area and proposes a mechanism for radical decomposition via reactions between the Keggin ions and radical species.

A 25 μm film of PolyHPA was used for the fuel cell testing. The performance of the 50 cm^2 fuel cell was first tested in a H_2/O_2 environment at 80°C using saturated inlet gases, see data in Figure 2. The HFR was much greater than previously observed, as the electrodes were not hot pressed on to the film to avoid fracturing the membrane, and can also be attributed to unoptimized interfaces between the GDEs and the membrane, as the GDEs use Nafion as the ionomer and the membrane is solely PolyHPA. The HFR under these conditions was ca. 200 mΩ cm^2, which is high for a 25 μm film. An HFR value of ca. 54 mΩ cm^2 was previously achieved for a fuel cell fabricated from a 48 μm film of this same material and with the same electrodes.[26]

Once the initial fuel cell performance data was collected, an OCV hold AST was initiated to test the chemical degradation of the fuel cell.

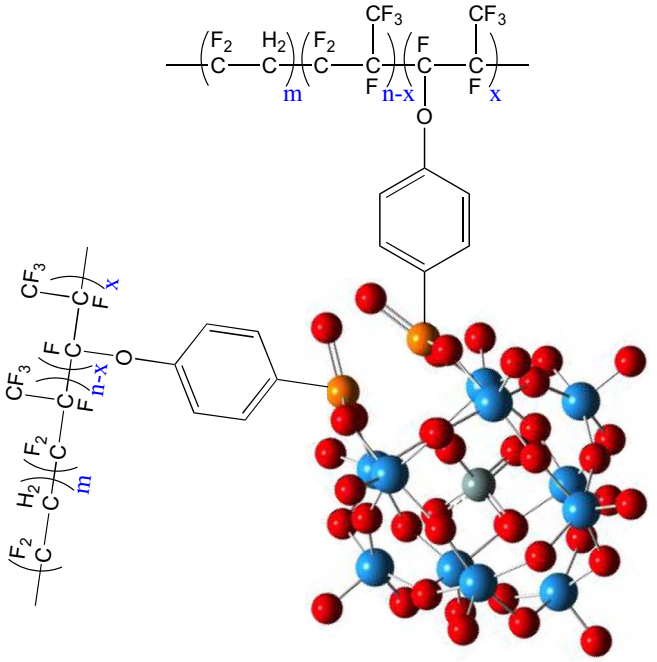

Figure 1. Structure of silicotungstic acid functionalized poly(vinylidene fluoride-co-hexafluoropropylene) (PolyHPA) reproduced with permission from the Royal Society of Chemistry from Ref. 26.

The voltage decay over time can be seen in Figure 3. The Department of Energy (DOE) target for a 500 h OCV hold is <20% voltage loss and <15 mA cm^{-2} of H_2 crossover. The target of <20% voltage loss was not achieved as the voltage loss was 26.5% with a decay rate of 520 μV h^{-1}, but the hydrogen crossover metric of <15 mA cm^{-2} was achieved (total current density at 0.4 V was ca. 10 mA cm^{-2}). It is important to remind the reader that no Ce or Mn have been added to this fuel cell and the electrodes still contain Nafion ionomer which would be subject to unmitigated chemical degradation. The OCV decay rate of the PolyHPA (25 μm, 520 μV h^{-1}, 0–500 h) is an improvement on that for Nafion N211 (25 μm, 2480 μV h^{-1}, 0–100 h) and a chemically durable hydrocarbon membrane (33 μm, 737 μV h^{-1}, 0–300 h).[18]

Next, the current density at 0.4 V in the LSV tests vs. time indicates that the first ca. 200 h did not show an increase in current. After that, the current density continually increased for the remainder of

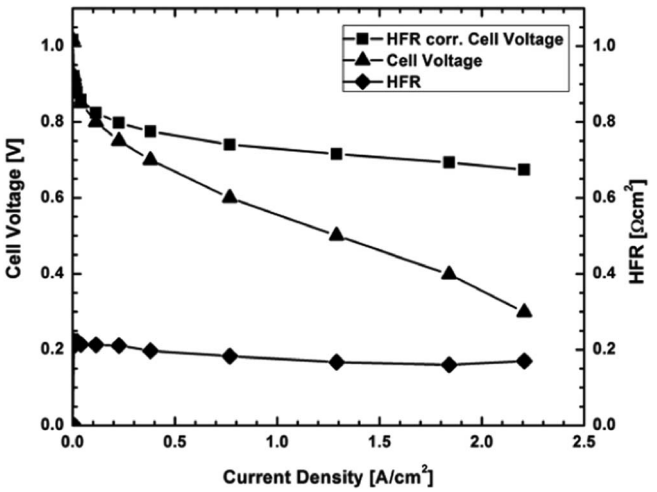

Figure 2. Fuel cell performance data at the beginning of the test at 80°C with saturated inlet gases operating with H_2/O_2.

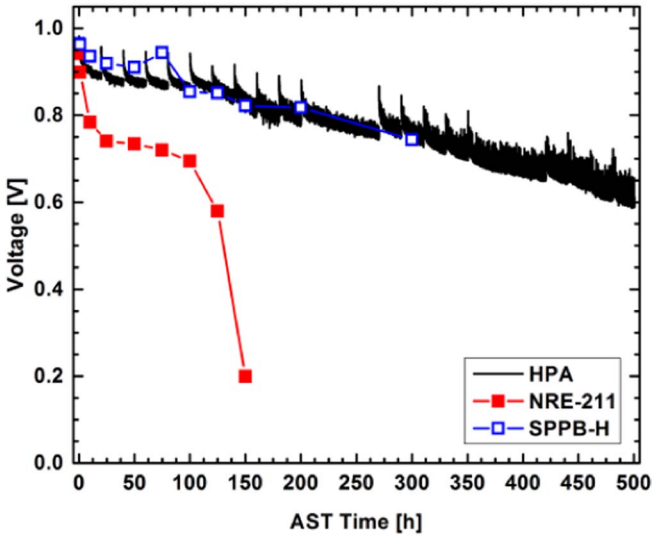

Figure 3. Cell voltage over time for the OCV hold test performed at 90°C, 30%RH, under H_2/Air, and an absolute pressure of 101.3 kPa. The HPA based film (-) had an initial voltage of 0.98 V and a final voltage of 0.72 V. Data for Nafion 211 (NRE-211) (■) and a sulfonated phenylated polyphenylene membrane (SPPB-H) (□) are shown for comparison. The NRE-211 and SPPB-H data has been reprinted from Ref. 18 with permission from John Wiley and Sons.

the test. The data, with lines to guide the eyes, can be seen in Figure 4. Even further insight can be gained through deconvolution of the contributions from electronic and hydrogen crossover. Through fitting the LSV data to a line between 0.25 and 0.50 V, the electronic resistance can be calculated as the inverse of the slope. The data is then corrected to remove the electronic resistance to obtain the hydrogen crossover contribution. Individual crossover contributions at 90°C and 30%RH can be seen in Figure 5. The hydrogen crossover is ca. 2 mA cm^{-2} or less for the whole test. This metric passes the DOE target of 15 mA cm^{-2} after 500 h of OCV hold. It then becomes evident that the failure mechanism of this fuel cell was the development of an electrical short, leading to the increased current observed in the LSV tests after 200 h. Near the end of the test, the deconvolution of electronic and hydrogen crossover results in negative values. While the exact values of the hydrogen and electronic crossover become less accurate

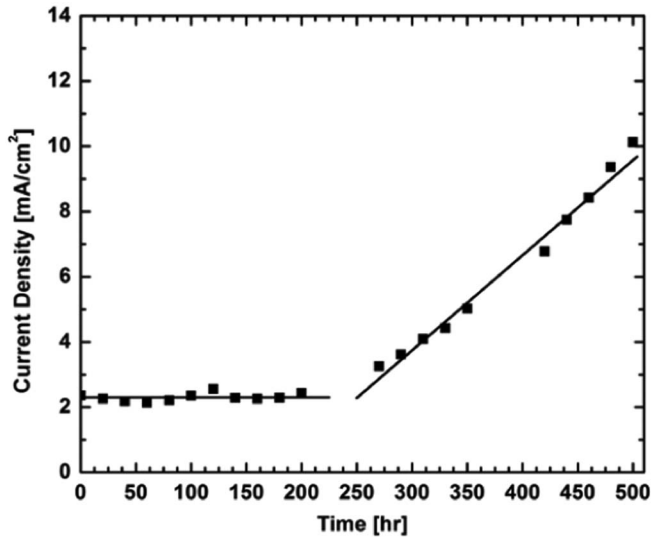

Figure 4. Crossover current at 0.40 V for the LSV test at different points throughout the OCV hold.

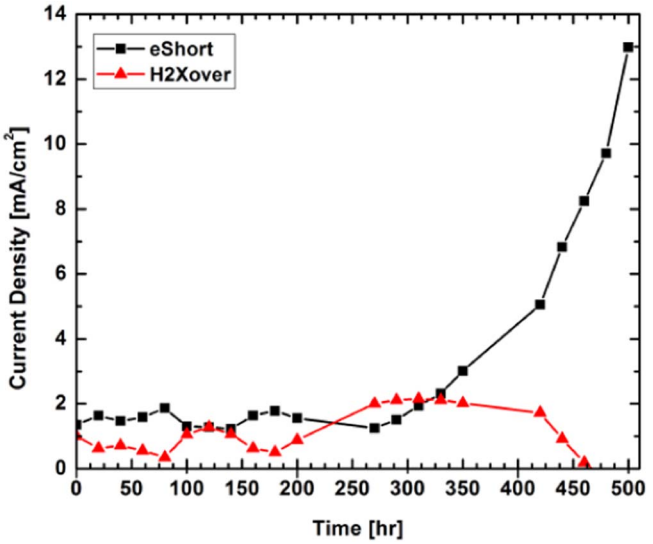

Figure 5. Different elements of crossover during the OCV hold.

and even erroneous toward the end of the test, the trend of increasing electronic crossover is believed to be accurate. This evidence indicates that the failure of this fuel cell was due to an electronic short, common for thin fuel cell membranes utilized without mechanical support.

Another factor that is worth noting is the relatively low HFR. The initial HFR was ca. 200 mΩ cm^2 at 80°C and 100%RH and only increased to ca. 500 mΩ cm^2 at 90°C and 30%RH. An HFR increase of only 150% is unusual between these two conditions, and provides further evidence that the high initial HFR is likely due to the resistance of an interface. Additional improvements are expected if this material is mechanically supported to mitigate voltage loss from electronic shorting, but this effort is outside the scope of this work.

Proposed radical scavenging mechanism.—Two advantages of this chemical stabilization approach are realized. First, the radical scavenging moiety is immobilized and thus will not suffer from migration. The second advantage is through using an acid that scavenges radicals, a high HSiW content results in a high concentration of both radical scavenging species and also mobile protons, two properties that are mutually exclusive with traditional chemical stabilization techniques.

The HSiW used in the membrane for the OCV hold test was organically hybridized through covalent attachment of phosphonic acid groups, but the rest of the HSiW moiety does not drastically change.[31] It is, therefore, assumed that the 11 terminal oxygen atoms in the hybridized form of the HSiW will have similar properties to the 12 terminal oxygen atoms in the Keggin structure and the only difference in reactivity will be the different number of reactive sites.

The rate of radical scavenging has a dependence on the concentration of the radical scavenging species in addition to the reaction rate constant. The rate constants for the most relevant reactions from the literature[32,33] with hydroxyl radicals can be seen in Table I and many more are extensively tabulated in other publications.[12,34,35]

The rate constant for Ce(III) is fast (3×10^8 L mol^{-1} s^{-1}), but reactions between HPA and hydroxyl radicals can be an order of magnitude faster. It is well known that WO_3 is able to readily and reversibly undergo changes in the oxidation state of W and the same is true for the W atoms in HPAs.[36,37] The $SiW_{12}O_{40}^{-5}$ anion is formed at −0.04V vs. NHE when excess protons are present, but this species is unlikely to exist in an operating fuel cell.[38] Both Reactions 6 and 7 involve the reduced form of the HPA reacting with hydroxyl radicals. While no rate data has been reported for the HSiW analogue of Reaction 5, it is conceivable that one exists.

To provide further evidence reaction enthalpies were calculated using DFT. It is proposed that one of the W atoms in HSiW may

Table I. Rate constants for reactions with hydroxyl radicals * PSSA is poly (p-sodium styrene sulfonate) ** PFSA decomposition is from trifluoroacetate.

Reaction	Rate	Reference
[1] PSSA + •OH → Decomposition	$k = 4 \times 10^8$ L mol^{-1} s^{-1}	Ref. 32
[2] PFSA + •OH → Decomposition	$k = <1 \times 10^6$ L mol^{-1} s^{-1}	Ref. 39
[3] Ce(III) + •OH + H^+→ Ce(IV) + H_2O	$k = 3 \times 10^8$ L mol^{-1} s^{-1}	Ref. 40
[4] Mn(II) + •OH + H^+→Mn(III) + H_2O	$k = 3 \times 10^7$ L mol^{-1} s^{-1}	Ref. 41
[5] $P_2W_{18}O_{62}H^{6-}$ + •OH→ $P_2W_{18}O_{62}{}^{6-}$ + H_2O	$k = 3 \times 10^9$ L mol^{-1} s^{-1}	Ref. 42
[6] $P_2W_{18}O_{62}{}^{7-}$ + •OH→Products	$k = 3 \times 10^{11}$ L mol^{-1} s^{-1}	Ref. 42
[7] $SiW_{12}O_{40}{}^{-5}$ + •OH + H^+→ $SiW_{12}O_{40}{}^{-4}$ + H_2O	$k = >1 \times 10^9$ L mol^{-1} s^{-1}	Ref. 33

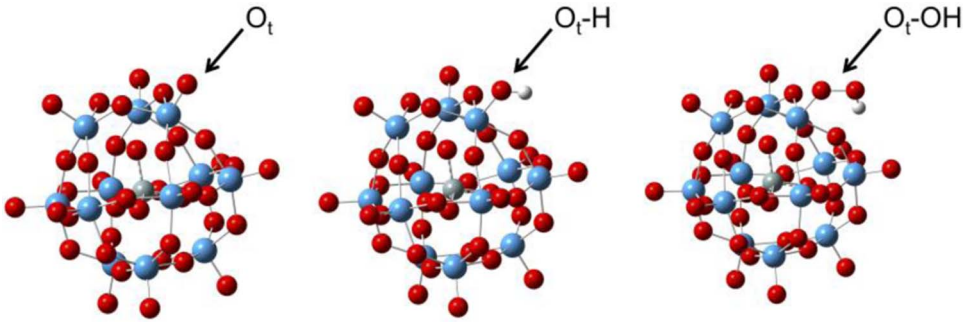

Figure 6. The optimized structures for (left) $[SiW_{12}O_{40}{}^{-4}]$, (middle) $[SiW_{12}O_{40}{}^{-4}]$-H, and (right) $[SiW_{12}O_{40}{}^{-4}]$-OH.

exist in two different oxidation states, W(VI) = O_t and W(V)-O_t-H or W(V)-O_t-OH, where O_t represents a terminal oxygen. The optimized structures of these hypothesized structures can be seen in Figure 6, and the assigned charges in the supplemental information, Figures S1–S3, with the coordinates in Tables S1-S3. Table II contains a tabulation of relevant properties near the active centers of the W octahedra. From this we can see that the rest of the Keggin anion is practically unaffected by the changes of one O_t and it is therefore expected that these findings are relevant to the organically functionalized lacunary HSiW moiety existing within the material discussed above (see structure in Figure 1).

When a radical species is added to the Keggin anion, the W-O_t bond is lengthened from 1.72 Å in the Keggin structure to 1.93 and 1.92 Å in the $[SiW_{12}O_{40}{}^{-4}]$-H and $[SiW_{12}O_{40}{}^{-4}]$-OH structures, respectively. The geometry and charge for the $[SiW_{12}O_{40}{}^{-4}]$-OH intermediate is similar to that of H_2O_2, with the exception of the dihedral which is 142.9° (H-O-O-H) for H_2O_2 and −5.0° (W-O_t-O-H) for the $[SiW_{12}O_{40}{}^{-4}]$-OH intermediate. The H atom appears to be interacting with the adjacent negatively charged oxygen atom.

Table II. DFT optimized bond lengths, angles, dihedrals, and Mulliken charge near the terminal oxygen (O_t). *H_2O_2 values are given for comparison.

	$SiW_{12}O_{40}{}^{-4}$	$SiW_{12}O_{40}H^{-4}$	$SiW_{12}O_{40}OH^{-4}$	H_2O_2*
W-O_t (Å)	1.72	1.93	1.92	-
O_t-H (Å)	-	0.98	-	-
O_t-O (Å)	-	-	1.49	1.48
O-H (Å)	-	-	1.00	0.98
W-O_t-H (°)	-	116.0	-	-
W-O_t-O (°)	-	-	119.5	100.8
W-O_t-O-H (°)	-	-	−5.0	142.9
W (Mulliken charge)	2.063	1.930	1.950	-
O_t (Mulliken charge)	−0.530	−0.767	−0.443	−0.404
H (Mulliken charge)	-	0.404	0.458	0.404

The reaction enthalpies for several plausible reactions with •H, •OH, •OOH, and O_2[8–15] were calculated using the energy of these optimized structures and can be seen in Table III. The energies were calculated in vacuum, with no solvent (implicit or explicit) consideration, no acidic protons, and using effective core potential basis sets, all of which will result in some error in the results and, therefore, we will discuss the trends and not emphasize the precise values obtained in the calculations.

The reaction of the Keggin anion with a hydrogen radical or a hydroxide radical can be seen in Reactions 8 and 9, respectively. The combination reaction of the Keggin anion with a hydrogen radical is exothermic (ca. −50 kcal mol^{-1}) while the reaction with the hydroxide radical is slightly endothermic (ca. +10 kcal mol^{-1}). Next, the Reactions 10–13 show that the reaction of the $[SiW_{12}O_{40}{}^{-4}]$-H intermediate with •H, •OH, •OOH, and O_2 are all exothermic (between −40 and −70 kcal mol^{-1}) and regenerate the Keggin anion. Note that only the reaction with O_2 generates a new radical species. The remaining Reactions 14 and 15 in Table III involve the $[SiW_{12}O_{40}{}^{-4}]$-OH intermediate reacting with •H and •OH to regenerate the initial Keggin anion and are both exothermic ca. −130 and −60 kcal mol^{-1}, respectively. The theoretical reaction enthalpies for different pathways involving the $[SiW_{12}O_{40}{}^{-4}]$-H and $[SiW_{12}O_{40}{}^{-4}]$-OH intermediate can be seen in Figure 7 and Figure 8, respectively. The formation of $[SiW_{12}O_{40}{}^{-4}]$-H is exothermic, likely serving as the intermediate in the radical decomposition mechanism. It is possible that $[SiW_{12}O_{40}{}^{-4}]$ is better at neutralizing hydrogen radicals that have been identified as the species responsible for chain scission.[11]

Improved radical scavenging efficiency.—In addition to the rate constants, the concentration plays a pivotal role in the overall reaction rate. One main benefit of using radical scavenging acids is the ability to achieve high concentrations of radical scavenging species without reducing the number of mobile protons. A simple calculation is best able to demonstrate this. The molar concentration of HSiW in a film with 70 wt% HSiW and 30 wt% polymer backbone can be calculated, as seen in Equation 1.

$$0.70 \frac{g\ HSiW}{g\ poly} * 3400 \frac{g\ Poly}{L\ Poly} * 3.1 * 10^{-4} \frac{mol\ HSiW}{g\ HSiW} = 0.74\ M\ HSiW \quad [1]$$

Table III. Reaction enthalpies from DFT calculations.

Reaction	Calculated Energy
[8] $[SiW_{12}O_{40}^{-4}] + {}^{\bullet}H \rightarrow [SiW_{12}O_{40}^{-4}]$-H	−49.6 kcal/mol
[9] $[SiW_{12}O_{40}^{-4}] + {}^{\bullet}OH \rightarrow [SiW_{12}O_{40}^{-4}]$-OH	11.0 kcal/mol
[10] $[SiW_{12}O_{40}^{-4}]$-H + ${}^{\bullet}OH \rightarrow [SiW_{12}O_{40}^{-4}] + H_2O$	−66.1 kcal/mol
[11] $[SiW_{12}O_{40}^{-4}]$-H + $O_2 \rightarrow [SiW_{12}O_{40}^{-4}] + {}^{\bullet}OOH$	−46.8 kcal/mol
[12] $[SiW_{12}O_{40}^{-4}]$-H + ${}^{\bullet}OOH \rightarrow [SiW_{12}O_{40}^{-4}] + H_2O_2$	−40.4 kcal/mol
[13] $[SiW_{12}O_{40}^{-4}]$-H + ${}^{\bullet}H \rightarrow [SiW_{12}O_{40}^{-4}] + H_2$	−59.0 kcal/mol
[14] $[SiW_{12}O_{40}^{-4}]$-OH + ${}^{\bullet}OH \rightarrow [SiW_{12}O_{40}^{-4}] + H_2O_2$	−57.2 kcal/mol
[15] $[SiW_{12}O_{40}^{-4}]$-OH + ${}^{\bullet}H \rightarrow [SiW_{12}O_{40}^{-4}] + H_2O$	−126.7 kcal/mol

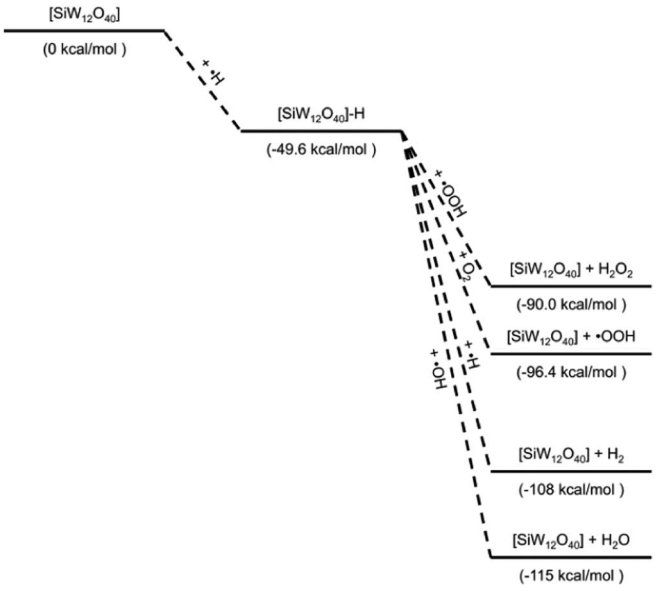

Figure 7. Possible reactions involving the $[SiW_{12}O_{40}^{-4}]$-H intermediate with the relative enthalpies in kcal/mol.

A similar value for replacing 10% of the protons in Nafion can be calculated, as seen in Equation 2.

$$0.00091\frac{mol\ H^+}{g\ poly} * 2000\frac{g\ Poly}{L\ Poly} * 0.33\frac{mol\ Ce^{3+}}{mol\ H^+} * 10\% = 0.06\,M\,Ce \quad [2]$$

Comparing Eqs. 1 and 2 indicates that over an order of magnitude greater concentration of HSiW is contained in a PolyHPA film with a loading of 70 wt% when compared to the concentration of Ce^{3+} in a PFSA membrane. Next, the rates can be calculated from the product of concentration of radical scavenging species and the associated rate constants.

$$\left(0.06\,M\,Ce^{3+}\right)^* \left(3^*10^8 M^{-1}s^{-1}\right) = 2^*10^7 s^{-1} \quad [3]$$

$$(0.7\,M\ HSiW)^* \left(>1^*10^9 M^{-1}s^{-1}\right) = >7^*10^8 s^{-1} \quad [4]$$

This calculation results in the potential for >35X increase in rate of decomposition of •OH. This alone is impressive by itself, but another huge advantage is that the covalently attached HSiW should not be able to migrate, therein solving one of the challenges experienced with the current technology.

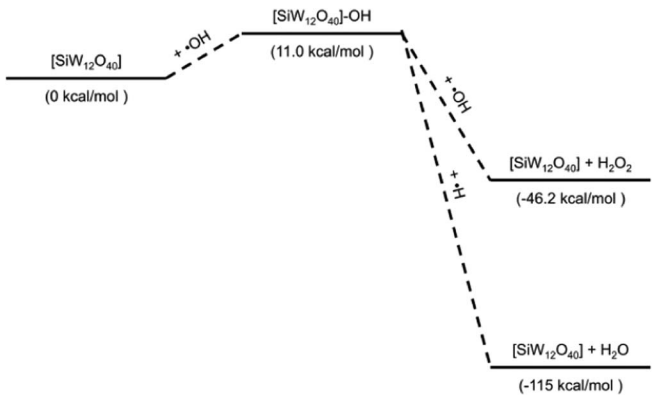

Figure 8. Possible reactions involving the $[SiW_{12}O_{40}^{-4}]$-OH intermediate with the relative enthalpies in kcal/mol.

Conclusions

The chemical stability of a 25 μm PolyHPA membrane was tested with an OCV accelerated stress test (H_2, Air, 90°C, 30%RH) and demonstrated outstanding chemical stability with a decay rate 520 μV h^{-1}. The fuel cell suffered an electrical short after 200 h, resulting in increasing current density in the LSV crossover test, indicating mechanical support is needed for the practical use of this material.

The literature was reviewed for rate constants for reactions of HPAs with radicals and indicates that the rate constant for radical decomposition can be over an order of magnitude faster for HSiW than for Ce or Mn. DFT calculations were performed and thermochemistry arguments were used to develop two plausible reaction networks for radical decomposition and scavenger regeneration, with the most likely mechanism involving a $[SiW_{12}O_{40}^{-4}]$-H intermediate. The calculations were used to demonstrate how the higher concentration of HPA (ca. 0.7 M) could result in even more advantages for radical scavenging, as the overall rate depends on both concentration and rate constant.

Future work should include mechanical support of thin membranes to avoid electrical shorting, incorporation of PolyHPA into the electrodes to reduce interfacial transport resistances arising from Nafion/PolyHPA interfaces, and studies on combined chemical and mechanical stress testing to probe the effects of migration. Lastly, the mechanism should be verified experimentally. The use of covalently tethered HSiW offers many benefits over traditional radical mitigation strategies and warrants further study.

Acknowledgments

The authors acknowledge the Fuel Cell Technology Office of the US Department of Energy, Energy Efficiency and Renewable Energy for funding under a grant DE-EE0006363.

ORCID

Andrew M. Herring https://orcid.org/0000-0001-7318-5999

References

1. C. C. Chan, *P Ieee*, **95**, 704 (2007).
2. T. Larriba, R. Garde, and M. Santarelli, *Int J. Hydrogen Energ*, **38**, 2009 (2013).

3. A. M. Herring and V. Di Noto, *Interface magazine*, **24**, 37 (2015).
4. T. E. Springer, T. A. Zawodzinski, and S. Gottesfeld, *J. Electrochem. Soc.*, **138**, 2334 (1991).
5. Y.-H. Lai, K. M. Rahmoeller, J. H. Hurst, R. S. Kukreja, M. Atwan, A. J. Maslyn, and C. S. Gittleman, *J. Electrochem. Soc.*, **165**, F3217 (2018).
6. M. Zatoń, J. Rozière, and D. J. Jones, *Sustainable Energy & Fuels*, **1**, 409 (2017).
7. A. Kusoglu and A. Z. Weber, *Chem Rev*, **117**, 987 (2017).
8. S. Shi, A. Z. Weber, and A. Kusoglu, *J. Membr. Sci.*, **516**, 123 (2016).
9. F. D. Coms, *ECS Trans.*, **16**, 235 (2008).
10. A. A. Shah, T. R. Ralph, and F. C. Walsh, *J. Electrochem. Soc.*, **156**, B465 (2009).
11. L. Ghassemzadeh, T. J. Peckham, T. Weissbach, X. Luo, and S. Holdcroft, *J. Am Chem Soc*, **135**, 15923 (2013).
12. L. Gubler, S. M. Dockheer, and W. H. Koppenol, *J. Electrochem. Soc.*, **158**, B755 (2011).
13. A. M. Baker, R. Mukundan, D. Spernjak, E. J. Judge, S. G. Advani, A. K. Prasad, and R. L. Borup, *J. Electrochem. Soc.*, **163**, F1023 (2016).
14. A. M. Baker, S. K. Babu, R. Mukundan, S. G. Advani, A. K. Prasad, D. Spernjak, and R. L. Borup, *J. Electrochem. Soc.*, **164**, F1272 (2017).
15. Andrew M. Baker, S. T. D. Williams, R. Mukundan, D. Spernjak, S. G. Advani, A. K. Prasad, and R. L. Borup, *J. Mater Chem A*, **5**, 15073 (2017).
16. M. Yandrasits, M. Lindell, D. Peppin, A. Komlev, S. Hamrock, G. Haugen, E. Fort, and K. Kalstabakken, *J. Electrochem. Soc.*, **165**, F3261 (2018).
17. L. Gubler, T. Nauser, F. D. Coms, Y.-H. Lai, and C. S. Gittleman, *J. Electrochem. Soc.*, **165**, F3100 (2018).
18. M. Adamski, T. J. G. Skalski, B. Britton, T. J. Peckham, L. Metzler, and S. Holdcroft, *Angewandte Chemie*, **129**, 9186 (2017).
19. J. L. Malers, M.-A. Sweikart, J. L. Horan, J. A. Turner, and A. M. Herring, *Journal of Power Sources*, **172**, 83 (2007).
20. G. M. Haugen, F. Meng, N. V. Aieta, J. L. Horan, M.-C. Kuo, M. H. Frey, S. J. Hamrock, and A. M. Herring, *Electrochem Solid St*, **10**, B51 (2007).
21. R. Paul Brooker, L. J. Bonville, and D. K. Slattery, *J. Electrochem. Soc.*, **160**, F75 (2012).
22. K. S. Mason, K. C. Neyerlin, M. C. Kuo, K. C. Horning, K. L. More, and A. M. Herring, *J. Electrochem. Soc.*, **159**, F871 (2012).
23. J. L. Horan, A. Genupur, H. Ren, B. J. Sikora, M.-C. Kuo, F. Meng, S. F. Dec, G. M. Haugen, M. A. Yandrasits, S. J. Hamrock, M. H. Frey, and A. M. Herring, *ChemSusChem*, **2**, 193 (2009).
24. J. L. Horan, A. Lingutla, H. Ren, M.-C. Kuo, S. Sachdeva, Y. Yang, S. Seifert, L. F. Greenlee, M. A. Yandrasits, S. J. Hamrock, M. H. Frey, and A. M. Herring, *J. Phys Chem C*, **118**, 135 (2013).
25. A. R. Motz, M.-C. Kuo, and A. M. Herring, *ECS Trans.*, **80**, 565 (2017).
26. A. R. Motz, M.-C. Kuo, J. L. Horan, R. Yadav, S. Seifert, T. P. Pandey, S. Galioto, Y. Yang, N. V. Dale, S. J. Hamrock, and A. M. Herring, *Energ Environ Sci*, **11**, 1499 (2018).
27. Y. Zhao and D. G. Truhlar, *Theoretical Chemistry Accounts*, **120**, 215 (2008).
28. P. J. Hay and W. R. Wadt, *The Journal of Chemical Physics*, **82**, 299 (1985).
29. Gaussian 09, M. J. Frisch, G. W. Trucks, H. B. Schlegel, G. E. Scuseria, M. A. Robb, J. R. Cheeseman, G. Scalmani, V. A Barone, B. Mennucci, G. A. Petersson, H. Nakatsuji, M. Caricato, X. Li, H. P. Hratchian, A. F. Izmaylov, J. Bloino, G. Zheng, J. L. Sonnenberg, M. Hada, M. Ehara, K. Toyota, R. Fukuda, J. Hasegawa, M. Ishida, T. Nakajima, Y. Honda, O. Kitao, H. Nakai, T. Vreven, J. A. Montgomery Jr., J. E. Peralta, F. O. Ogliaro, M. J. Bearpark, J. Heyd, E. N. Brothers, K. N. Kudin, V. N. Staroverov, R. Kobayashi, J. Normand, K. Raghavachari, A. P. Rendell, J. C. Burant, S. S. Iyengar, J. Tomasi, M. Cossi, N. Rega, N. J. Millam, M. Klene, J. E. Knox, J. B. Cross, V. Bakken, C. Adamo, J. Jaramillo, R. Gomperts, R. E. Stratmann, O. Yazyev, A. J. Austin, R. Cammi, C. Pomelli, J. W. Ochterski, R. L. Martin, K. Morokuma, V. G. Zakrzewski, G. A. Voth, P. Salvador, J. J. Dannenberg, S. Dapprich, A. D. Daniels, Ã. D. N. Farkas, J. B. Foresman, J. V. Ortiz, J. Cioslowski, and D. J. Fox, Gaussian, Inc., Wallingford CT, 2016.
30. R. Signer and H. Gross, *Helvetica Chimica Acta*, **17**, 1076 (1934).
31. G. S. Kim, K. S. Hagen, and C. L. Hill, *Inorg. Chem.*, **31**, 5316 (1992).
32. Y. K. Bhardwaj, H. Mohan, S. Sabharwal, and T. Mukherjee, *Radiat. Phys. Chem.*, **62**, 229 (2001).
33. M. Kim, I. A. Weinstock, Y. V. Geletii, and C. L. Hill, *Acs Catal*, **5**, 7048 (2015).
34. G. V. Buxton, C. L. Greenstock, W. P. Helman, and A. B. Ross, *Journal of Physical and Chemical Reference Data*, **17**, 513 (1988).
35. L. Gubler and W. H. Koppenol, in *The Chemistry of Membranes Used in Fuel Cells: Degradation and Stabilization*, S. Schlick, Editor, p. 107 (2017).
36. T. Yamase, *Chem Rev*, **98**, 307 (1998).
37. F.A. Cotton and G. Wilkinson, *Advanced Inorganic Chemistry* 5th edition, Wiley-Blackwell (1988).
38. P. Gómez-Romero and N. Casañ-Pastor, *The Journal of Physical Chemistry*, **100**, 12448 (1996).
39. P. Maruthamuthu, S. Padmaja, and R. E. Huie, *Int J. Chem Kinet*, **27**, 605 (1995).
40. R. W. Matthews, *Aust J. Chem*, **37**, 475 (1984).
41. M. Pick-Kaplan and J. Rabani, *The Journal of Physical Chemistry*, **80**, 1840 (1976).
42. B. G. Ershov, N. L. Sukhov, N. I. Kartashev, and V. I. Spitsyn, *Bulletin of the Academy of Sciences of the USSR Division of Chemical Science*, **30**, 952 (1981).